Available online at www.sciencedirect.com
ScienceDirect
Journal of the European Ceramic Society 30 (2010) 2859–2870
www.elsevier.com/locate/jeurceramsoc

Co-extrusion of multilayered ceramic micro-tubes for use as solid oxide fuel cells

Jonathan Powell [a,*], Stuart Blackburn [b,c]

[a] Department of Metallurgy and Materials Science, The University of Birmingham, UK
[b] Department of Chemical Engineering, The University of Birmingham, UK
[c] Interdisciplinary Research Center in Materials Processing, The University of Birmingham, UK

Available online 3 March 2010

Abstract

Current methods to manufacture tubular solid oxide fuel cells (SOFCs) involve multiple steps of extrusion, layer deposition and sintering, leading to high manufacturing costs. The aim of the work presented in this paper is to reduce the cost of manufacturing SOFCs. This is achieved by developing a method for manufacturing a five-layered micro-tubular structure by a multi-billet co-extrusion process. With the implementation of continuous screw extrusion equipment, this co-extrusion process could easily be adapted into a fully continuous manufacturing process.

The co-extrusion process presented initially involves rheologically unifying five pastes made up of individual powder compositions. It is shown that it is possible to formulate the pastes with in an optimum solids loading region where the die land rheological properties are relatively insensitive to small variations in solids loading, thus allowing for a more stable process.

These pastes are then extruded as billets from separate extrusion barrels through a single nozzle. This uses a novel die design which does not require the use of a central mandrel to form the tubular structure. The sintered structure comprises four Ni/YSZ anode layers and a YSZ electrolyte layer, each layer being approximately 60 μm thick, forming a tube with an outer diameter of 3 mm and an inner diameter of 2.4 mm.

Keywords: Extrusion; Fuel cells; Shaping; Micro-tube; Composites

1. Introduction

Solid oxide fuel cells (SOFCs) are considered to offer a highly efficient, environmentally friendly solution to the growing problem of providing sustainable power generation for the future. Fuel cells electrochemically convert the chemical potential energy contained in fuels directly into electrical potential energy. They work in a similar manner to batteries, except that fuel cells are designed to be continuously replenished with the reactants as they are consumed, and their electrodes are catalytic and are therefore not consumed. Fuel cells are typically designed to run on hydrogen, but can be run on other fuels.

There are a variety of fuel cells available, but those of interest here are SOFCs, which are in essence a combination of functional ceramics. The SOFC uses a non-porous ceramic material as the electrolyte, which is typically zirconia that only permits the transfer of oxygen ions. The anode and the cathode are usually made of porous ceramic and cermet materials, through which electrons, gases and ions can travel. The most common materials used for the anode and cathode material are NiO/YSZ cermets and strontium doped lanthanum manganite respectively. However many other materials, such as gandolinia doped ceria (electrolyte)[1] or lanthanum nickel ferrite (cathode),[2] may be considered where co-processing is being proposed.

SOFCs come in two main forms; a planar design where the fuel cells are stacked together or as tubular structures as shown in Fig. 1, a design for a fuel cell unit proposed by Alston et al.[3] Current planar manufacturing methods involve adding layers onto a prefabricated anode or cathode support. This allows for the manufacture of thin electrolyte layers, helping to improve the power density of the fuel cell. However these methods require many processing and sintering steps, increasing the production costs of the fuel cell. Self supporting SOFCs use much thicker electrolytes, but co-processing potentially allows manufacture to be carried out in fewer steps, as the electrolyte can be manufactured and sintered with the anode and/or the cathode.

Co-sintering presents its own problems due to thermo-physical incompatibilities between the materials. During

* Corresponding author. Tel.: +44 7525941060; fax: +44 121 4143441.
E-mail address: jdapowell@hotmail.com (J. Powell).

0955-2219/$ – see front matter © 2010 Elsevier Ltd. All rights reserved.
doi:10.1016/j.jeurceramsoc.2010.02.010

cooling, residual stresses in the SOFC structure can cause cracking due to differences in thermal expansion and thermal expansion rates. It is therefore important to match materials, so that these stresses are minimized. One method of doing this is to use a functionally graded design, where there is continuous compositional change across a layer. Here, the authors approximate a functionally graded system with multiple layers each with an incremental change in composition. As well as reducing the thermal and residual stresses this structure also increases the number of triple phase sites, where the electrons, gas and ions meet to electrochemically react.

The manufacture of a multilayered self supported tubular SOFC in a single manufacturing step also poses its own difficulties. The co-extrusion of multiple pastes requires fine tuning and unification of the paste rheologies in order to prevent the formation of flow defects and to allow the use of continuous extrusion. This, therefore, requires the formulation of a number of pastes containing powders with differing particle sizes, size distributions, morphologies and surface chemistries, as well as pore size, distribution and shape. Previous work by Liang and Blackburn,[4,5] Zhang et al.,[6] Chen et al.[7] and others has looked at the co-extrusion of multilayered tubes. These tubes were relatively large, with layer thicknesses being in the order of 1 mm, a limitation which the authors believe could be overcome by a change in design of the co-extrusion process and equipment. Some of these authors also reported the formation of delamination defects, which again the authors believe can be overcome by improved design of the co-extruder.

This paper summarises the development of a process to manufacture micro-tubular solid oxide fuel cells by multi-billet co-extrusion of rheologically unified pastes, which form the YSZ electrolyte and the NiO/YSZ anode. The process initially involves rheologically unifying the five paste formulations. A paper previously published by the authors[8] showed that the required liquid content for pastes made from different powder mixtures can be predicted to give a series of pastes with unified rheologies. This was done by estimating the packing density of the individual powders, using information gathered from the change in rheological properties with the paste solids loading (solids volume fraction). Using the packing the density of the individual powders, the packing density of mixed powder systems were then predicted using an extended Westman model.[9]

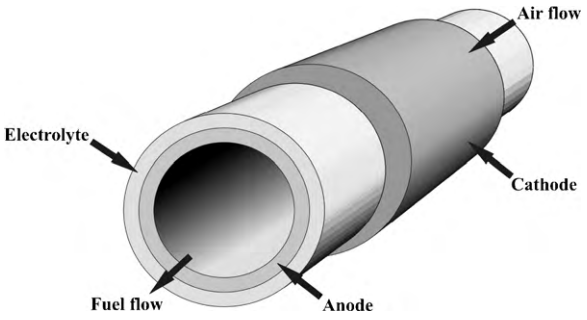

Fig. 1. Schematic of a self supporting SOFC and its proposed use in a domestic combined heat and power unit.[3]

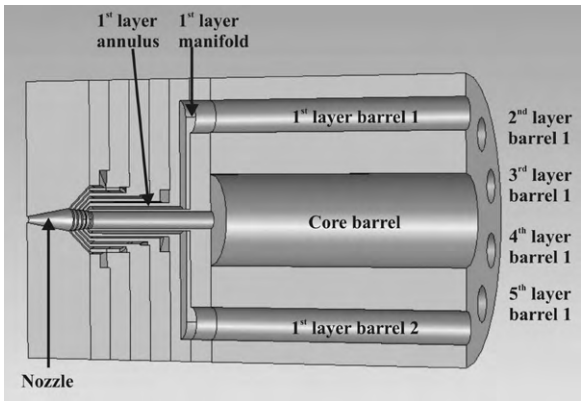

Fig. 2. Cross sectional view of the co-extruder.

Co-extrusion tooling has been designed to manufacture a five-layered tubular structure, giving a functionally graded structure that is designed to reduce the residual thermal stresses between the electrolyte and anode layers. In order to achieve the small dimensions required for a micro-tube, the authors have incorporated the use of a sacrificial core paste replacing a solid mandrel, thus eliminating the possibility of damaging this part of the die and reducing the shear rate in the this part of the die.

2. Co-extruder design

The co-extruder was designed to manufacture rods with five outer layers, where the central core material can be a sacrificial material allowing for the formation of tubular structures upon the removal of that core material. In order to achieve this co-extruded rod structure, the pastes were supplied from separate barrels into their respective flow fields, made up of manifolds and concentric annuli. The main features of the co-extruder and the paste flow paths are illustrated in Figs. 2 and 3.

The extrusion pressure was supplied by means of a universal load frame which applied a load to the individual extrusion barrels via a transition plate at a constant cross head speed, resulting in a controlled flow rate for each paste.

The co-extruder was designed to transfer six pastes from their respective barrels into a system of a core and five laminate layers. The separate barrels were contained within a single unit, with the barrel for the core material being surrounded by the barrels for the five layers. The central core of the co-extrudate was formed via the first die, comprising a flat plate with an attached central thin walled tube through which the core material could flow, the outer wall acted as the central mandrel for the adjacent or next layer. The five layers were fed from their barrels to five consecutive plates, each containing a manifold (transition slot) that transferred the incoming material from the outer inlet holes, around the central mandrel formed by the previous die into the outlet annulus formed by the attached thin walled tube and the previous thin walled die.

As with any co-extrusion process, it is important to ensure that all flow streams exit the die at a constant and unified velocity. This prevents the formation stresses between the layers and deformation and instability of the co-extruded green part. To

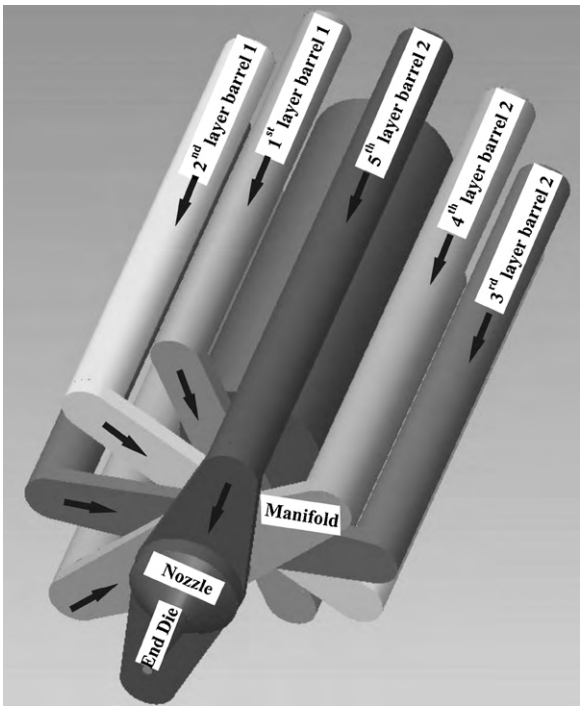

Fig. 3. Paste flow paths in the co-extruder.

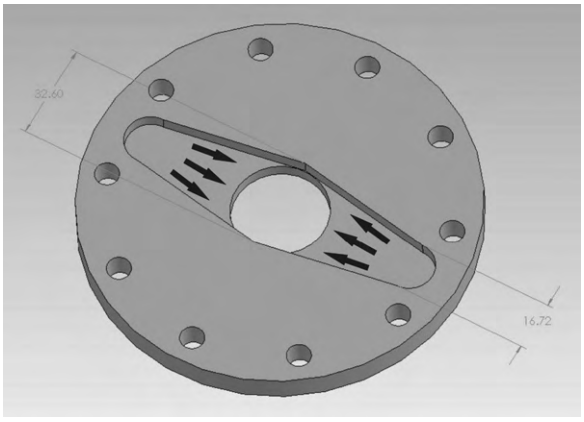

Fig. 4. Illustration of a manifold showing the increase in width of channel to accommodate the large annulus diameter. The paste is forced outwards to evenly spread the flow at the annulus entry by decreasing the height of the manifold and its cross sectional area.

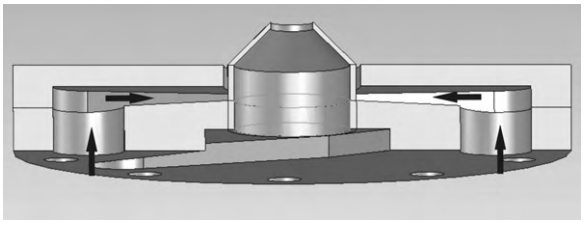

Fig. 5. Illustration of the manifold cross section from the side showing the decrease in the manifold height. This is designed to spread the flow of the paste evenly across the manifold thus allowing it to enter the annulus at a constant flow rate throughout its circumference.

ensure a unified extrudate velocity, the ratio between the barrel and nozzle exit cross sectional areas was kept constant for all six flow fields. By fixing the dimensions of the nozzle according the required co-extrudate geometry, the barrels were designed such that the ratio of the barrel to the nozzle cross sectional area (A_0/A) was equal to 2.66×10^{-3} for all flow fields.

2.1. Co-extruder features for improved performance

In transferring the pastes from their barrels into the concentric annuli, it was necessary for the material to flow around a mandrel, possibly leading to poor filling of the volume around the mandrel and subsequent flow defects in the co-extrudate. This becomes a particular problem as the diameter of the mandrel becomes increasingly large. In order to overcome this issue each layer was fed by two barrels positioned diametrically opposite each other. This ensured that the paste could completely fill the circumference of the mandrel as illustrated in Figs. 4 and 5. This design feature could also lead to improved binding at the interfaces between the combining streams around a mandrel due to increased pressures at the interface. Another advantage to this design feature is that the loads on the device are more effectively balanced, thus reducing the possibility of failure due to twisting of the co-extruder.

Another feature incorporated into the co-extruder was the use of a constantly decreasing cross sectional area in all the flow fields. This feature aims to reduce the formation of laminations and poorly filled or deformed co-extrudate geometries as a result of the non-uniform extrusion velocities throughout the flow field cross section. One section of the co-extruder where this feature played an important role was within the manifolds, where some of the mandrels were considerably larger in diameter than the diameter of the manifold inlet. To force the material to spread out evenly across the manifold, the height of the manifold channel was decreased as the width increased to accommodate for the large diameter mandrel, such that the cross sectional area decreased in the direction of flow. Figs. 4 and 5 illustrate how the manifold design features promote even flow of the paste into the annulus.

Another important feature of this co-extruder and process is the use of a sacrificial core to enable the manufacture of tubular structures. One of the advantages of using this method instead of the conventional fixed central mandrel are that much smaller tubes can be manufactured, as there is no issue of damaging the mandrel. In fact with this method there is no lower limit to the inner diameter of the tube, as long as there is adequate pressure and the co-extruder can accommodate this load. Another advantage is that with out the mandrel there is no inner die wall, which can contribute to the deformation of the laminar structure of the co-extrudate. Fig. 6 illustrates the design of the nozzle and the use of a sacrificial core to replace the mandrel for producing a tubular structure.

3. Co-extruder pressure models

In designing the co-extruder the pressure drop across the tool was predicted. This ensured that once manufactured it would be possible to extrude the formulated pastes at the required velocity. The pressure drop was modelled for the purpose made fuel

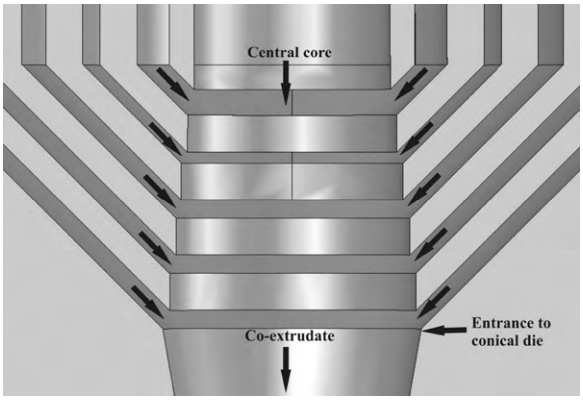

Fig. 6. Co-extruder nozzle design using a core paste instead of a mandrel, which if a sacrificial material is used will produce a tubular structure.

cell pastes using the rheological data obtained from Benbow Bridgwater analyses.[10,11]

The model treats the co-extruder as a series of simple die entries and die lands, making it possible to model the pressure drop using a generalised version of the six parameter Benbow Bridgwater equation[11];

$$P = P_1 + P_2 = (\sigma_0 + \alpha' V^m) \ln\left(\frac{A_0}{A}\right) + \left(\frac{ML}{A}\right)(\tau_0 + \beta' V^n) \quad (1)$$

where P_1 represents the pressure due to die entry flow and P_2 represents the pressure due to die land flow. The parameters σ_0 and τ_0 represent the bulk and die wall initial yield stress respectively, α and β are the die entry and die land velocity factors and m and n are the velocity exponents. A_0 is the die entry or barrel cross sectional area, A is the die land cross sectional area, M is the die land perimeter and L is the die land length.

The co-extruder pressure model splits up each flow field into defined regions, the barrel, manifold, annulus, conical annulus and cone. As well as the geometrical sections, the co-extruder was split into distinct flow regions in terms of pressure, the manifold entry (P_I) and die land (P_{II}), the annulus entry (P_{III}) and die land (P_{IV}), the nozzle die land (P_V) and the conical die land (P_{VI}), such that the total pressure across the co-extruder is equal to the sum of the pressure across the separate segments. The total pressure drop across a single flow field, which represents the flow path of single layer, up until the layers combine at the end of the conical annulus nozzle, is given by the following equation;

$$P_F = P_I + P_{II} + P_{III} + P_{IV} + P_V \quad (2)$$

where P_F is the pressure drop across a single flow field up to the end of the conical annulus. The total pressure drop across the co-extruder for all flow fields (all extruded layers) is as follows;

$$P_T = \sum_{i=0}^{5} (P_I + P_{II} + P_{III} + P_{IV} + P_V)_i + P_{VI} \quad (3)$$

where P_T is the total pressure drop across the whole extruder when all the layers are being co-extruded and i is the layer number, where 0 is the central core, 1 is the inner layer, working outwards to 5 which is the outer layer of the tube.

The manifold and annuli pressure drops can be predicted using the generalised form of the Benbow Bridgwater equation, shown by Eq. (1). Models derived for the conical annulus and conical die were resolved using numerical and integral solutions, which are denoted by the subscripts *num* and *int* respectively. Benbow and Bridgwater have previously derived an integral solution of their equation for the pressure drop across the conical die for solid rod manufacture and is as follows[11];

$$P_{VI\text{int}} = 2(\sigma_0 + \alpha' V^m + \tau_0 \cot\theta) \ln\left(\frac{D_{CO}}{D_C}\right) + \frac{\beta' V^n}{n}\left[1 - \left(\frac{D_C}{D_{CO}}\right)^{2n}\right] \cot\theta \quad (4)$$

where D_{C0} and D_C are the inlet and outlet diameters of the conical die and θ is the die entry angle normal to the axis of flow, where for a square entry die, $\theta = 90^\circ$.

A new numerical solution for the conical geometry was obtained using the rectangle rule. The results were compared to those of the integral solution provided by Benbow and Bridgwater. In this case the rectangle rule is used. This was done by treating the cone as a series of discrete steps such that the diameter of the cone decreases with increments of $2x$ for an axial displacement of x, the equations for which are as follows;

$$P_1 = \sum_{i=j}^{i=0} 2 \ln\left(\frac{D_0}{D_0 - 2ix_i}\right)\left(\sigma_0 + \alpha\left(\frac{Q}{\pi((D_0 - 2ix_i)/1)^2}\right)^m\right) \quad (5)$$

$$P_2 = \sum_{i=j}^{i=1} \left(\frac{4L}{D_0 - 2ix_i}\right)\left(\tau_0 + \beta\left(\frac{Q}{\pi((D_0 - 2ix_i)/1)^2}\right)^n\right) \quad (6)$$

where P_1 represents the pressure drop due to die entry flow, P_2 represents the pressure due to die land flow, D_0 is the inner diameter at the entry to the conical annulus and Q is the paste flow rate.

In order to predict the pressure drop across the conical annulus nozzle, new integral and numerical solutions were derived using the method adopted by Benbow and Bridgwater.[11] Fig. 7 shows a schematic diagram of the conical annulus nozzle and the definition of some of the terms used in the integral solution for this geometry. As can be seen in Fig. 7, the model disregards the pressure drop due to the entry and exit zones as these are non-symmetric regions along the axis of flow, and are therefore difficult to model using this method. The new solution derived using the method described in 'Paste Flow and Extrusion'[11] is as follows;

$$dP = \int_{0.5D\cot\theta}^{0.5D_0\cot\theta} \left(-\frac{2\tau_0 \sin\theta}{c} - 2\beta \sin\theta\left(-\frac{Q \tan\theta \sin\theta}{\pi c^2(2zc + c^2)}\right)^n\right) dz \quad (7)$$

where c is the distance between the walls of the conical annulus, measured parallel to the axis of the co-extruder. θ denotes the angle of the conical annulus, where a 45° angle would represent

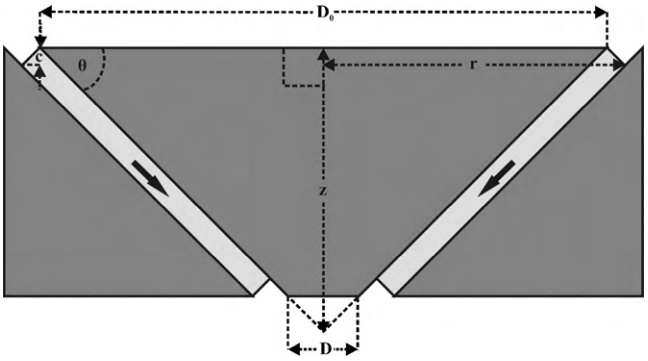

Fig. 7. Schematic diagram of the conical annulus nozzle, showing the definition of terms for the pressure model integral solution for this geometry.

a parallel annulus, z denotes the axial distance from the conical annulus entrance to the exit. Refer to Fig. 7 for a diagrammatical definition of the terms in Eq. (7).

As with the conical die, the pressure drop across the conical annulus also obtained using a numerical solution; in this case the rectangle rule was used. Fig. 8 illustrates the numerical model of the conical annulus and defines some of the variables. The equations for the pressure due to die entry flow (P_1) and die land flow (P_2) are as follows;

$$P_1 = \sum_{i=j}^{i=0} 2 \ln \left(\frac{(D_{0,1} - 2ix)^2 - (D_{0,2} - 2ix)^2}{(D_{0,1} - 2(i+1)x)^2 - (D_{0,2} - 2(i+1)x)^2} \right) \times \left(\sigma_0 + \alpha \left(\frac{4Q}{\pi((D_{0,1} - 2(i+1)x)^2 - (D_{0,2} - 2(i+1)x)^2)} \right)^m \right) \quad (8)$$

$$P_2 = \sum_{i=j}^{i=1} \left(\frac{2(D_{0,1} + D_{0,2})(i+1)x^2}{(D_{0,1} - 2(i+1)x)^2 - (D_2 - 2(i+1)x)^2} \right) \times \left(\tau_0 + \beta \left(\frac{4Q}{\pi((D_{0,1} - 2(i+1)x)^2 - (D_2 - 2(i+1)x)^2)} \right)^n \right) \quad (9)$$

where $D_{0,1}$ and $D_{0,2}$ are the outer and inner diameters at the inlet to the conical annulus, and x is the increment size.

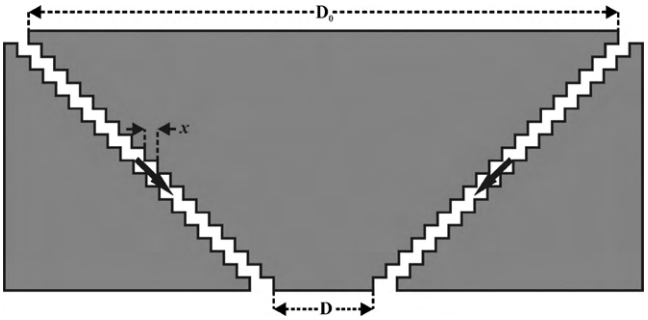

Fig. 8. Schematic diagram representing the numerical solution for the model of the conical annulus.

Table 1
Sintered tube layer compositions.

Layer		YSZ (%, v/v)	NiO (%, v/v)
Electrolyte		100	0
Anode	A	80	20
	B	60	40
	C	40	60
	D	20	80

4. Paste formulation, preparation and rheological analysis

In order to successfully co-extrude a series of pastes, the flow properties of the materials must be unified such that flow, structure and geometry defects are minimised or eliminated. Differences in flow behaviour, in particular bulk flow behaviour, i.e. the flow characterised by the material entering the die: can result in the preferential deformation and strain of one of the pastes and therefore a change in the relative flow velocities of the co-extruding materials. This localised preferential strain of a given paste in the co-extruded system can result in axial or radial cracks depending on the mode of strain. If undergoing extensional flow, the compliant material will preferentially undergo extensional plastic deformation, whilst the incompliant material will crack radially across the laminar layer.

The manufactured tubes were made of five layers each with a different composition of yttria stabilised zirconia and nickel, designed for use as solid oxide fuel cells. The five layers were designated as four Ni/YSZ anodic layers and a single YSZ electrolyte layer. As such, the pastes used to produce the layers of the tube had varying compositions of NiO and YSZ. To introduce porosity into the anode layers carbon black powder was also added to their corresponding pastes, and for the manufacture of the sacrificial core used to produce the final tubular structure, a paste containing only carbon black as the solid phase was formulated.

The powders were mixed thoroughly in the dry state prior to wetting. The liquid was added to the powder and the material was then transferred to a twin roll mill. The material was mixed for a total of 15 min and the paste was finally removed as a sheet and rolled into rods ready for laying up into the extruder. This mixer is particularly effective at breaking up powder agglomerates to give highly homogenous systems. This is done by adjusting the rollers on the mixer to a very small gap size, providing very strain rates and ensuring that the mixing energy is transferred more effectively to the agglomerated particles. The pastes were formulated to give sintered tubes with the compositions shown in Table 1.

The corresponding powder volume fractions in the pastes, taking into account the addition of carbon black for the formation of pores in the sintered rod, are shown in Table 2.

4.1. Materials

The electrolyte paste was prepared using an yttria stabilized zirconia powder HSY8 (Daiichi Kigenso Kagaku Kogyo Co.,

Table 2
Powder volume fractions in the co-extruded pastes.

Paste	NiO (v/v)	YSZ (v/v)	C (v/v)
1	0.00	1.00	0.00
2	0.14	0.69	0.30
3	0.28	0.52	0.30
4	0.42	0.34	0.30
5	0.56	0.17	0.30

Japan), which has an average particle size of 0.5 μm. The anode pastes were made up as mixtures of HSY8, black nickel oxide (−325 mesh, Cerac, USA), and Monarch 120 carbon black (Cabot, UK), which acted as a pore forming agent. A proprietary organic binder system (Functional Materials Group, University of Birmingham, UK) was used. The organic binder was made from an organic solvent, polymer binder, plasticiser and lubricant. As the binder system was a developmental formulation, no brand name or further description can be provided.

4.2. Paste rheological analysis

The paste rheological parameters were evaluated by extrusion capillary rheometry using a ram extruder driven by a compression load frame, as shown in Fig. 9. The ram extruder consists of a ram, a 20.00 mm diameter barrel and a series of interchangeable dies 4.00 mm in diameter, with lengths 4.00, 16.00 and 32.00 mm.

The extrusion rate was controlled by adjusting the cross head speed, giving extrudate velocities ranging from 5.00 to 0.13 mm s^{-1}. The pressure was recorded for each extrudate velocity and the data was then used to characterise the pastes by applying the Benbow Bridgwater six parameter model, shown by Eq. (10), modified specifically to model the flow through circular shaped dies and die entries;

$$P = P_1 + P_2 = 2(\sigma_0 + \alpha' V^m) \ln\left(\frac{D_0}{D}\right) + \left(\frac{4L}{D}\right)(\tau_0 + \beta' V^n) \tag{10}$$

where P is the total pressure drop and P_1 and P_2 are the pressure drop due to convergent flow and plug flow respectively. D_0 is the barrel diameter and D is the die diameter.

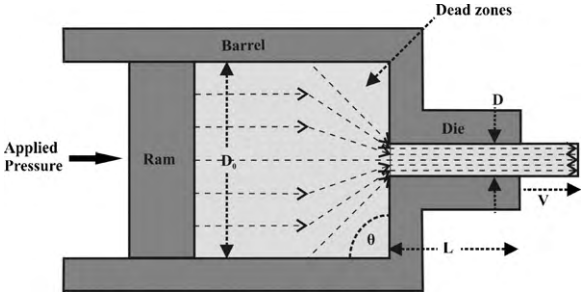

Fig. 9. Ram extrusion of a paste, where D_0 is the barrel diameter, D is the die diameter, L is the die length, θ is the die entry angle and V is the extrudate velocity.

4.3. Mixed powder packing

All five pastes used in the co-extrusion process were made from varying compositions of three different powders. In order to obtain rheologically unified pastes, controlled volumes of liquid binder were added to the different powder mixtures. Previous work by the authors has shown the paste rheology can be adjusted and controlled by making controlled additions of the binder over above the critical binder volume fraction.[8] The critical binder volume fraction is defined as the binder content required for filling the packed powder bed voids without separating the powder particles.

This method requires prior knowledge of the powder packing density, which in this case was predicted by extrapolating rheological data from pastes with a range of solids loadings. It is assumed that for a paste made from a given powder system a critical solids loading exists, where by the binder contained in the paste insufficient to lubricate the flow of particles, preventing the powder particles from flowing. It is assumed that this critical solids loading represents the powder packing density of the powder system, as this is the condition in which the volume fraction of the liquid binder is only sufficient to fill the voids between the particles and no more. It has previously been shown that the relationship between the solids loading and the inverse of the extrusion pressure is approximately linear, with the intercept on the x axis representing the critical solids loading.[8] The packing density of the three component powders was therefore obtained by producing pastes of varying solids content and using rheological test information to predict the maximum solids loading of the paste. A more detailed account of this procedure is provided in a previously published paper of the authors.[8] Using an extended Westman powder packing model,[9] the packing density of the ternary powder mixtures was predicted. The equations used for these predictions are shown below:

$$1 = \phi_{m,i+1}^2 \left(\frac{1}{\phi_{\max,i}} - \frac{1 - x'_{i+1}}{\phi_{\max,i}}\right) + 2G_i \frac{\phi_{\max,i}\phi_{m,i+1}}{1 - \phi_{\max,i}} \times \left(\frac{1}{\phi_{\max,i+1}} - \frac{1 - x'_{i+1}}{\phi_{\max,i}}\right)\left(\frac{1}{\phi_{\max,i+1}} - 1 + x'_{i+1} - \frac{x'_{i+1}}{\phi_{m,i+1}}\right) + + \left(\frac{\phi_{\max,i}}{1 - \phi_{\max,i}}\right)^2 \left(\frac{1}{\phi_{\max,i+1}} - 1 + x'_{i+1} - \frac{x'_{i+1}}{\phi_{m,i+1}}\right)^2 \tag{11}$$

$$\forall \frac{d_{i+1}}{\bar{d}_i} \leq 0.824 : G_i = 0.738\left(\frac{d_{i+1}}{\bar{d}_i}\right)^{-1.57} \tag{12}$$

$$\forall \frac{d_{i+1}}{\bar{d}_i} > 0.824 : G_i = 1 \tag{13}$$

where $\phi_{\max,i}$ is the packing density of the coarse grain in the mixture (or pure coarse grain powder for a binary system), $\phi_{m,i+1}$ is the packing density of the fine grain material, $\phi_{\max,i+1}$ is the packing density of the coarse/fine mixture with a fine grain volume fraction of x'_{i+1}. G_i is a packing parameter and is a function of the particle size and shape, where $\bar{d}_i$ is the characteristic diameter of the mixture of coarse grain powders (or simply the characteristic diameter of the pure coarse grain powder for a binary system) and d_{i+1} is the particle diameter of the fine grain powder which is being added to the coarse grain powders.

The particle size of the powders (d) was analysed by initially forming pastes. The pastes were then mixed into a

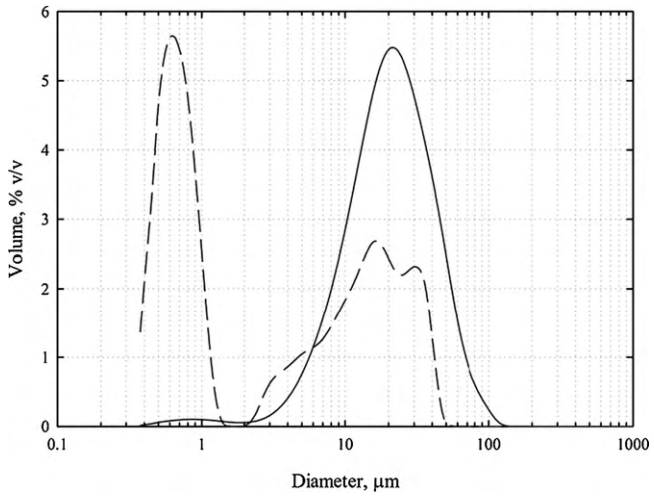

Fig. 10. Particle size distribution of carbon black; solid line—as received carbon black suspended in water, dashed line—processed carbon black suspended in cyclohexanone.

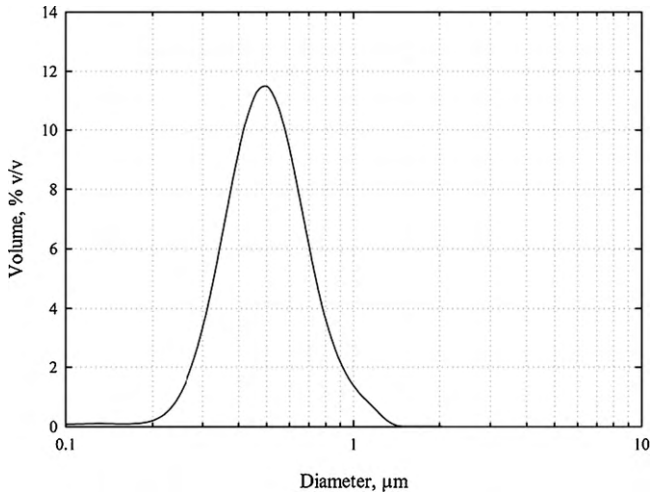

Fig. 12. Particle size distribution of YSZ.

dilute suspension/solution with cyclohexanone. The particles in the suspension were then analysed using laser diffractometry (Malvern Mastersizer 2000E). By analysing the particles from the preformed pastes, it was ensured that the powders were in a condition representative of their state during the manufacturing process. The results of the particle size analysis are represented in Figs. 10–12.

5. Co-extrusion of multilayered ceramic micro-tubes

Having developed and characterised the paste formulations, and verified the co-extruders capability and performance by means the pressure modelling and Play Doh (Hasbro Toys, US) extrusion, the six paste formulations were co-extruded, debound and sintered.

The extrusion was carried out using a universal load frame, with a 200 kN load cell and an extrudate velocity of 3 mm s^{-1}. The co-extrudates were formed with the electrolyte as the inside layer. To minimise the production of waste material, the volume of paste required to fill each flow field was calculated from the 3 dimensional drawings. From this the mass of the paste required to fill the co-extruder was calculated and added to mass required to produce the required length of co-extrudate.

The resulting co-extrudates were dried in an oven and the resulting dry extrudates were debound and sintered in a muffle furnace. The sintered rods were reduced within a 1% hydrogen atmosphere in a tube furnace. The temperature profiles used for the drying, debinding and sintering are given in Table 3.

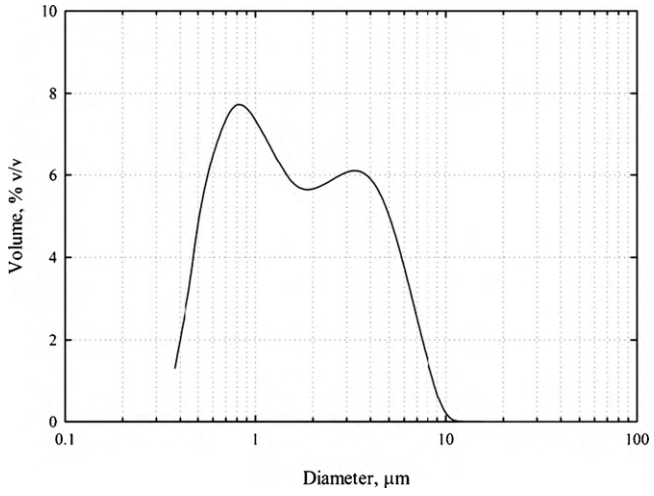

Fig. 11. Particle size distribution of NiO.

6. Results and discussion

6.1. Powder size analysis

Fig. 10 shows the particle size distribution of the carbon black powder. The solid line represents the size distribution of the pre-processed powder when suspended in water, the dotted line represents data obtained for the pre-processed powder when suspended in the solvent used for the paste binder. The mean particle sizes of the powder in water and cyclohexanone are 21.00 and 3.00 μm respectively. The curves show that the powder clearly disperses more effectively in the cyclohexanone.

Fig. 10 indicates that the carbon black powder has a much larger particle size than would be expected. According to Cabot the primary particle size of Monarch 120 carbon black is a few nanometers in diameter. However these particle form agglomerates which are strongly bonded by physical bonds, these agglomerates form weakly bonded flocculants. The multimodal nature of the powder as shown in Fig. 10 is likely to be a result of these flocculants being broken down into the agglomerates. As the powder was twin roll milled in a paste form for both the powder size analysis and the co-extrusion paste preparation, we can expect this particle size distribution to be representative of the carbon black particle size distribution in the co-extruded pastes. However the Westman model assumes that the particles are solid with an approximately spherical shape, which in these test conditions is a false assumption.

Table 3
Co-extrudate post extrusion processing temperature profiles.

	Temp. 1 (°C)	Rate 1 (°C min^{-1})	Temp. 2 (°C)	Dwell 2 (h)	Rate 2 (°C min^{-1})	Temp. 3 (°C)	Dwell (h)
Drying	RT	1	150	5	2	RT	0
Debinding	RT	5	400	0	1	600	5
Sintering	600	5	1350	2	2	RT	0
Reduction	RT	5	200	5	5	RT	0

Table 4
Packing densities for the YSZ, NiO and carbon black powders.

Powder	Packing density (v/v)
YSZ	0.57
Carbon	0.55
NiO	0.52

Fig. 11 shows the distribution of the NiO powder particles which has a bi-modal distribution with a mean particle size of 1.52 μm. The bi-modal distribution of the NiO and carbon black powders could lead to difficulties in obtaining reliable results from the powder packing predictions, particularly if the mean particle size changes as a result of processing.

Fig. 12 shows the size distribution of the YSZ powder, having a Gaussian mono-modal distribution indicating the powder is fully dispersed and deagglomerated. The mean particle size of the particles is 0.51 μm and the particle size distribution is relatively narrow. The small particle size should assist in preventing phase migration during extrusion, and the high dispersibility of the particles should lead to fewer defects and improved mixing of the powders in the extrudates. The narrow distribution of this fine powder will also lead to improved packing of the powder within the interstices of coarser powders.

6.2. Powder packing predictions

The packing densities of the individual powders, YSZ, NiO and carbon black, were estimated from the critical solids loadings of the pastes, which were measured from the relationship between the solids loading and the inverse die entry stress. The densities are given in Table 4.

The results of the powder packing predictions for the three powders are illustrated in Fig. 13; the powder mixtures for the co-extruded pastes are indicated by the dots. The chart shows that according to the predictions there is a range in volumetric powder packing densities between the powder mixtures of approximately 10%. According to the previously described assumptions, the difference in required volume fraction of binder for the highest and lowest powder mixture packing densities will be within the range of 10%, in order to obtain pastes with unified rheology. Based on these results, pastes were produced according to the formulations shown in Table 5.

6.3. Co-extrusion paste rheological analysis

The five pastes formulated for the co-extrusion process were rheologically analysed and compared. The extrusion pressure results are illustrated in Fig. 14 and provided in Table 6. Previously published work carried out by Van Hoy et al.,[12] indicated that variations in extrusion pressure of 5% can be tolerated between the co-extruded pastes without flow defects forming. The extrusion pressures fall within the 5% tolerance over the larger die lengths but the error becomes much larger, over 10%, for the short die length: $L/D = 1$. This implies that the pastes are rheologically matched in terms of die land plug flow behaviour, but they are less well matched in terms of the die entry bulk shear and extensional flow properties.

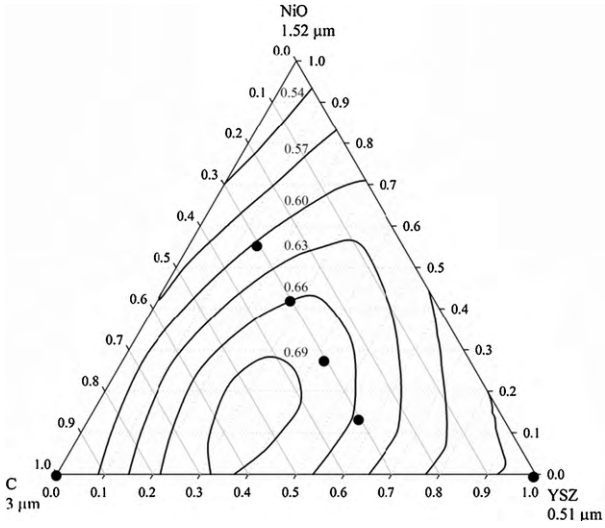

Fig. 13. Ternary mixture powder packing densities according to the extended Westman model.[9]

The rheological parameters calculated using the Benbow Bridgwater equation, are provided in Table 7. The parameters lead to similar conclusions drawn from the experimental extrusion pressures, indicating that the die entry flow properties are less well matched than the die land flow behaviour. They also show that for all the pastes, the extrusion pressure is dominated by die entry flow, indicated by a comparatively high die entry yield stress and velocity factor.

Table 5
Co-extrudate paste formulations.

Paste	Mass (g)			
	NiO	YSZ	C	Binder
1	0.00	198.38	0.00	23.38
2	50.22	183.70	33.88	26.40
3	105.05	144.10	35.44	26.40
4	150.65	91.85	33.88	26.40
5	155.22	35.49	26.18	26.40

Table 6
Extrusion pressures for co-extrusion pastes, $D = 4$ mm.

Extrudate velocity (mm s^{-1})		Extrusion pressure (MPa)					Average difference (%)
		Paste 1	Paste 2	Paste 3	Paste 4	Paste 5	
$L/D = 8$	5.00	49.11	44.25	47.75	44.56	46.52	3.50
	2.00	32.66	28.21	34.99	31.83	31.05	5.34
	1.00	25.05	22.29	25.02	25.61	24.34	3.75
	0.50	19.40	17.69	19.57	20.22	18.97	3.50
	0.25	14.80	14.23	15.58	16.27	14.79	4.18
	0.13	11.34	11.48	12.70	12.83	11.43	5.42
$L/D = 4$	5.00	27.25	30.34	28.65	28.41	31.61	4.72
	2.00	18.14	22.10	19.16	19.21	21.52	7.12
	1.00	14.01	15.60	15.19	14.96	16.59	4.32
	0.50	10.78	12.73	12.39	11.57	12.91	5.96
	0.25	9.07	10.19	9.99	9.20	10.10	4.74
	0.13	7.39	8.12	7.96	6.99	7.88	4.97
$L/D = 1$	5.00	14.64	17.51	16.74	15.45	13.40	8.11
	2.00	10.28	11.78	12.10	10.20	9.18	9.19
	1.00	7.95	8.89	9.76	8.28	7.12	8.81
	0.50	6.41	7.16	7.88	6.37	5.91	9.19
	0.25	5.21	5.98	6.53	5.41	4.61	10.20
	0.13	4.41	4.81	5.27	4.30	3.54	10.28

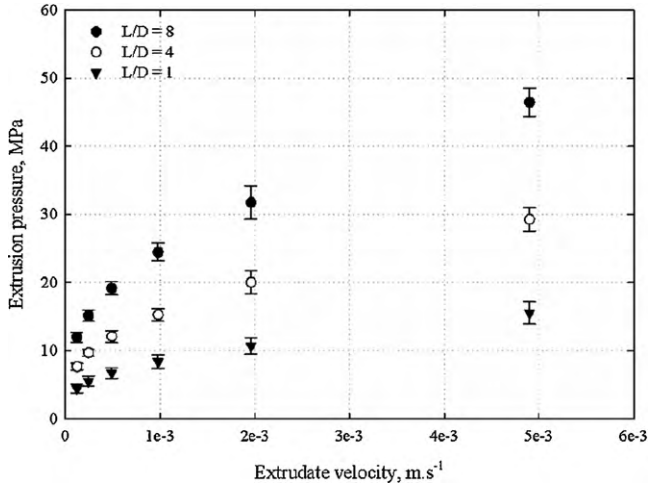

Fig. 14. Extrusion rheometry experimental pressures for the six co-extruded pastes, extruded through 3 dies with length/diameter ratios of 1, 4 and 8. The error bars represent the maximum and minimum extrusion pressures for the individual pastes tested.

The extrusion pressures predicted from these parameters for extrusion through a 4 mm diameter die are represented in Fig. 15. The relatively large range in predicted extrusion pressures compared to the experimental data can be attributed to accumulated errors associated with fitting the Benbow Bridgwater equation.

6.4. Predicted and experimental co-extrusion pressures

Using Eqs. (1)–(9) and the method previously described, the co-extrusion pressures were predicted for velocities ranging from 0.09 to 3.00 mm s^{-1}. Fig. 16 and Table 8 show the experimental and model co-extrusion pressure data. They show that the models provide a close approximation of the experimental data with the model prediction error ranging between 11 and 37%. The model error is defined as follows;

$$\%\text{error} = \left(\frac{\text{prediction} - \text{experiment}}{\text{experiment}}\right) \times 100 \quad (14)$$

The numerical model provides a more accurate prediction over this range of velocities with an average error of 24% compared to 34% for the integral model prediction. Regression was used to fit a three parameter power law equation to the data

Table 7
Benbow Bridgwater rheological parameters of co-extrusion pastes.

Paste	Benbow Bridgwater parameters					
	σ_0	α	m	τ_0	β	n
1	0.20	19.08	0.37	0.04	12.85	0.45
2	0.75	53.69	0.50	0.02	9.55	0.41
3	0.71	40.68	0.48	0.00	6.27	0.35
4	0.74	61.15	0.55	0.08	11.05	0.44
5	0.58	34.92	0.48	0.14	15.25	0.54

Table 8
Experimental and model co-extrusion pressure data.

Extrudate velocity (mm s^{-1})	Experimental pressure (MPa)	Integral model		Numerical model	
		Pressure (MPa)	%Error	Pressure (MPa)	%Error
3.00	29.46	39.90	35.44	36.59	24.20
1.50	23.65	31.27	32.25	28.89	22.20
0.75	19.35	25.52	31.92	23.69	22.45
0.35	16.13	21.35	32.35	19.87	23.16
0.19	13.38	17.97	34.36	17.40	30.08
0.09	11.20	15.39	37.40	13.85	23.71

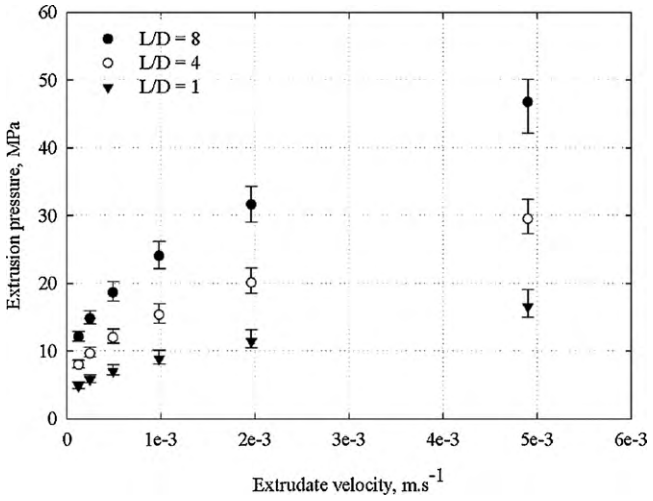

Fig. 15. Predicted extrusion rheometry pressures for the six co-extruded pastes using the Benbow Bridgwater model parameters in Table 6, for 3 dies with length/diameter ratios of 1, 4 and 8. The error bars represent the maximum and minimum predicted extrusion pressures.

points, providing a means of comparing the performance of the models against the experimental data.

$$y = y_0 + ax^b \tag{15}$$

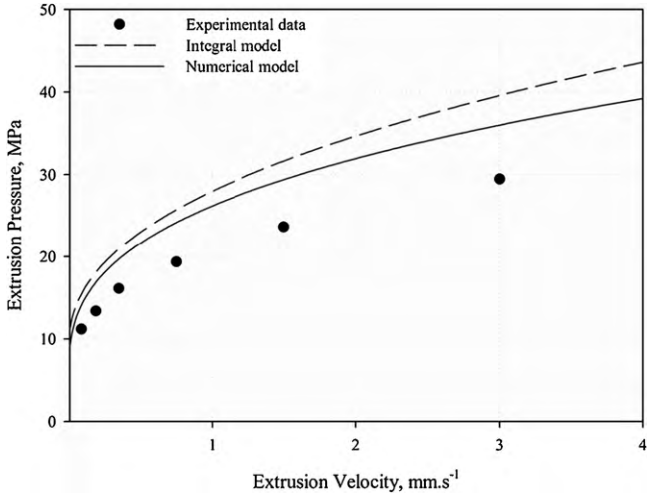

Fig. 16. Experimental and model co-extrusion pressure data with three parameter power law regression plots.

Table 9
Parameters obtained power law regression fit to model and experimental co-extrusion pressure data.

Power law parameters	Experimental data	Integral model	Numerical model
y_0	3.38	8.32	4.58
a	17.80	19.64	21.60
b	0.34	0.42	0.34

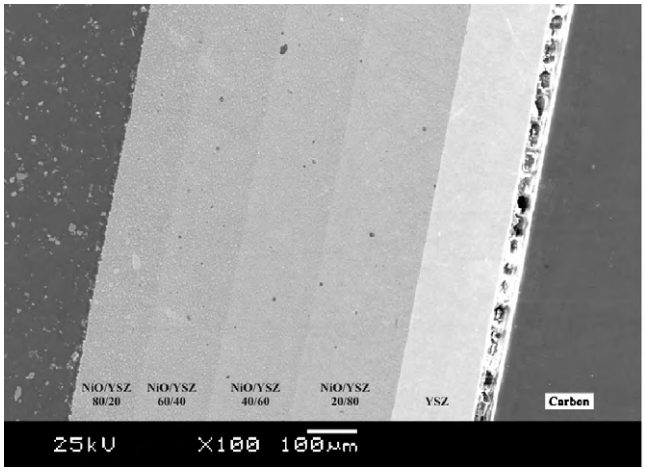

Fig. 17. Back scatter SEM image of the as extruded rods. The inner white layer being the YSZ layer, the outer grey layer is the 80/20 NiO/YSZ layer and the black region on the right is the carbon core paste.

The power law parameters shown in Table 9 indicate that the numerical model is more effective at predicting the shear thinning type behaviour of the pastes, implied by the well matched velocity exponents, b. The parameters also show that the numerical model is more effective at predicting the extrusion pressures at low velocities indicated by the closely matched intercepts on the y axis, y_0. These results show that under process conditions the numerical model is more effective at predicting the co-extrusion pressures. The numerical model provides a simpler calculation method, which may be useful with more complicated die geometries where integration can be impractical.

The Benbow Bridgwater model provides an effective and simple means for predicting extrusion pressures in complicated

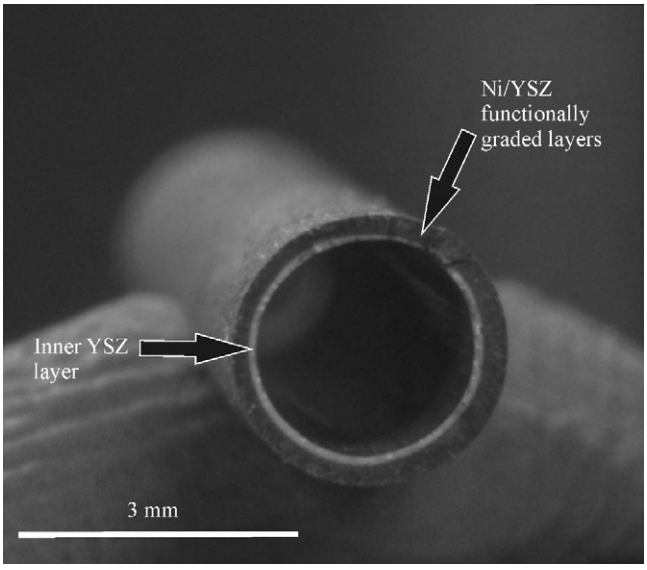

Fig. 18. Cross sectional view of ceramic micro-tube manufactured by co-extrusion showing the inner white YSZ layer surrounded by the four Ni/YSZ layers.

Fig. 19. Longitudinal view of ceramic micro-tube manufactured by co-extrusion showing the inner white YSZ layer surrounded by the four Ni/YSZ layers.

die geometries, providing the design engineer with the means to easily design co-extrusion tooling (Table 8).

7. Manufacture of multilayered ceramic micro-tubes

Fig. 17 shows a back scatter image of a dried co-extrudate clearly showing the presence of 5 distinct layers and a central core. This photograph represents a typical result after the drying of this co-extrudate structure. In the image large pores can clearly be seen, which could act as possible fracture origin sites. It is also clear that the layers are well adhered and defined with no sign of delamination, mixing or deformation of the laminar structure. As shown in Fig. 17, the dried co-extrudates consistently showed signs of delamination between the carbon layer and the inner YSZ layer. This is attributed to excessive differential shrinkage between the core and the outer five layers.

Figs. 18 and 19 show photographic images of the tube. The sintered product has held its tubular shape with good adhesion between the layers. Fig. 20 shows a secondary electron image of a typical sintered micro-tube cross section. Fig. 20 shows that in the reduced sintered state, the wall thickness is approximately 320 μm, with a YSZ layer thickness of approximately 84 μm. The inner YSZ layer is well defined by a clear and well bonded interface to the first nickel containing layer. The anode layers are less well defined in the sintered state but a gradual change in nickel content can be seen

Fig. 20 shows a porous structure throughout the anode layers, with the size of the pores appearing to increase with increasing Ni content. This appears to be linked to the growth of the nickel grains, in the form of NiO during sintering, which are shown be as large as 30 μm in the outer layer. The results of the mercury porositmetry on individual components show there is a loss in porosity with increasing Ni content. The images confirm this with some of the pores in the outer layer appearing not to be continuous or interconnected.

8. Conclusions

A process for manufacturing multilayered ceramic micro-tubes has been developed. The process involved developing and characterising co-extrusion pastes, designing a co-extrusion tool, modelling the co-extrusion pressures through that tool and finally producing a multilayered ceramic micro-tube. It was shown that useful predictions of the pressures required co-extrude pastes through complex dies could be made. An understanding of the design considerations with regards to complex die geometries was also gained and a tool built to allow future development of the co-extrusion process for producing micro-tubular solid oxide fuel cells.

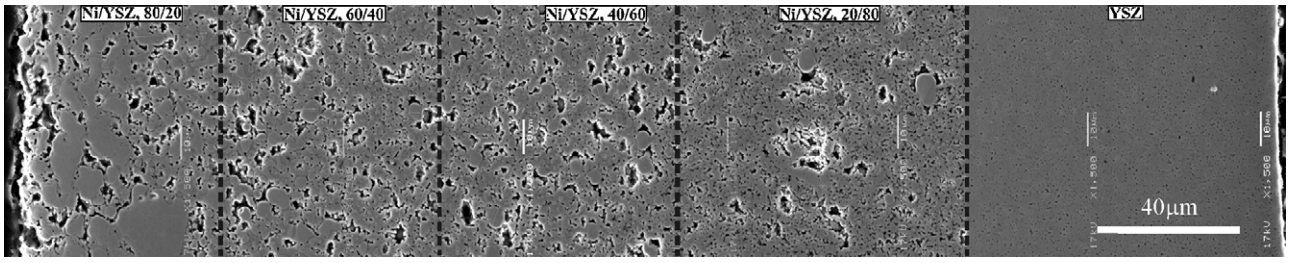

Fig. 20. Secondary electron image of a cross section of the reduced sintered co-extrudate.

References

1. Lee S, Lim Y, Lee EA, Hwang HJ, Moon J-W. *Journal of Power Sources* 2006;**157**:848–54.
2. Basu RN, Tietz F, Teller O, Wessel E, Buchkremer HP, Stöver D. *Journal of Solid State Electrochemistry* 2003;**7**:416–20.
3. Alston T, Kendall K, Palin M, Prica M, Windibank P. *Journal of Power Sources* 1998;**71**:271–4.
4. Liang Z, Blackburn S. *Journal of the European Ceramic Society* 2001;**21**:883–92.
5. Liang Z, Blackburn S. *Journal of Materials Science* 2002;**37**:4227–33.
6. Zhang W, Xie J, Wang C. *Materials Science and Engineering A* 2004;**382**:371–7.
7. Chen Z, Ikeda K, Murakami T, Takeda T, Xie J-X. *Journal of Materials Processing Technology* 2003;**137**:10–6.
8. Powell J, Blackburn S. *Journal of the European Ceramic Society* 2009;**29**:893–7.
9. Liu S, Ha Z. *Powder Technology* 2002;**126**:283–96.
10. Benbow JJ, Jazayeri SH, Bridgwater J. *Powder Technology* 1991;**65**:393–401.
11. Benbow JJ, Bridgwater J. *Paste flow and extrusion*. Oxford: Clarendon Press; 1993.
12. Van Hoy C, Barda A, Griffith M, Halloran JW. *Journal of the American Ceramics Society* 1998;**81**:152–8.